Research Square

Preprints are preliminary reports that have not undergone peer review.
They should not be considered conclusive, used to inform clinical practice,
or referenced by the media as validated information.

Dual-Time-Scale Economic Dispatch of Integrated Energy Systems Considering Dynamic Carbon-Cycle Constraints and Carbon-Budget Coordination

zhigang zhang

zhangzhigang@csg.cn

China Southern Power Grid (China)

junjie he

China Southern Power Grid (China)

Research Article

Keywords:

Posted Date: November 26th, 2026

DOI: https://doi.org/10.21203/rs.3.rs-11658384/v1

License: This work is licensed under a Creative Commons Attribution 4.0 International License.
Read Full License

Additional Declarations: No competing interests reported.

Dual-Time-Scale Economic Dispatch of Integrated Energy Systems Considering Dynamic Carbon-Cycle Constraints and Carbon-Budget Coordination

Junjie He[1] and Zhigang Zhang[1*]

[1]Guangzhou Nanfang Electric Power Group Electrical Technology Co., Ltd., Guangzhou, China.

*Corresponding author(s). E-mail(s): zhangzhigang@csg.cn;

Abstract

An integrated energy system (IES) with carbon recycling involves intertemporal inventory constraints and the allocation of daily carbon budgets. A six-inventory model is developed for CO_2-rich solvent, buffered CO_2, hydrogen, synthetic methane, battery energy, and thermal energy. The model explicitly represents carbon flows and energy consumption associated with capture, regeneration, electrolysis, methanation, and subsequent combustion. Building on day-ahead schedules, intraday receding-horizon optimization coordinates the remaining periods using realized emissions, current inventories, and forecast scenarios. A joint economic-quality certificate tests candidates for inventory-trajectory reuse; the full scenario problem is solved whenever a candidate fails certification. Validation uses public hourly energy-metering data from Kitakyushu and a common set of engineering retrofit assumptions. The test comprises 24 prespecified three-day windows in 2009–2010, totaling 72 operating days. Relative to conventional model predictive control (MPC), the proposed method reduces aggregate operating expenditure by approximately 0.81%, equivalent to approximately 8325 CNY, and operational CO_2 emissions by approximately 0.84%, while increasing end-to-end computation time by approximately 15.1%. Both methods satisfy their daily carbon budgets on 57 days. Under the engineering and forecasting conditions examined, the overall scheme improves average operating economics and emissions performance using common inventory-closure and carbon-budget accounting conventions.

Keywords: Integrated energy system, Dynamic carbon-inventory constraints, Daily carbon-budget coordination, Dual-time-scale dispatch, Multiday validation

1 Introduction

Carbon capture and power-to-gas (P2G) conversion enable an IES to transfer energy among electricity, heat, and gas while changing the timing of carbon storage in rich solvent, buffered CO_2, and synthetic methane. Regeneration and hydrogen production also consume energy: a low-expenditure decision in the current period can increase subsequent inventory-restoration requirements and carbon-budget compliance pressure. Economic dispatch therefore needs to track inventories, realized emissions, and the energy-supply conditions of the remaining periods, and to evaluate performance over consecutive operating days.

Liu et al. (2023) investigated dual demand response, tiered carbon trading, electricity–heat–gas storage, and day-ahead/intraday dispatch. Equations (28) and (29) of that study credit emissions reductions according to P2G operation. Building on this line of research, the present study explicitly models CO_2 sources, intertemporal carbon inventories, and the destination of synthetic methane, placing capture, utilization, and subsequent combustion within a consistent accounting boundary.

Previous studies have examined carbon-recycling dispatch (Zhang et al. 2022), multitime-scale carbon-allowance allocation with carbon capture, utilization, and storage (CCUS) (Shi et al. 2023), and electricity–heat–gas–hydrogen coupling with tiered carbon trading (Gao et al. 2025). Approaches to forecast uncertainty and online computational effort include distributionally robust adaptive MPC (Fan et al. 2024), stochastic MPC (Kumar et al. 2020), event-triggered economic MPC (Zhang et al. 2014; He et al. 2023), and early termination based on the duality gap (Pavlov et al. 2019). Coordination of multiple P2G units with seasonal storage (Marzi et al. 2024), multitime-scale coordination under dynamic carbon allowances (Liu et al. 2026), and control that decouples absorption and desorption through solvent storage (Qiu et al. 2025) provide foundations for intertemporal energy–carbon coordination. The present work integrates carbon-inventory evolution, daily carbon budgets, and forecast scenarios into a receding-horizon framework and evaluates expenditure, emissions, and computational effort over consecutive days.

The study addresses three connected aspects. First, a unified heating-value and carbon-atom accounting boundary represents six inventories and their dynamic coupling through capture, conversion, and combustion. Second, realized emissions, the remaining daily budget, and inventory states enter day-ahead/intraday coordination, with an economic-quality test determining whether a candidate trajectory can be reused. Third, prespecified three-day windows spanning different years evaluate overall operating performance.

2 System Boundaries and Dynamic Carbon-Cycle Constraints

Figure 1 summarizes the relationships among dynamic carbon-inventory constraints, daily carbon budgets, and dual-time-scale dispatch. The energy-supply and carbon-recycling components describe electricity–heat–gas coupling and carbon conversion

pathways; the control components link day-ahead scheduling, intraday receding-horizon optimization, and state feedback. Equipment and data boundaries are specified in Sect. 4.

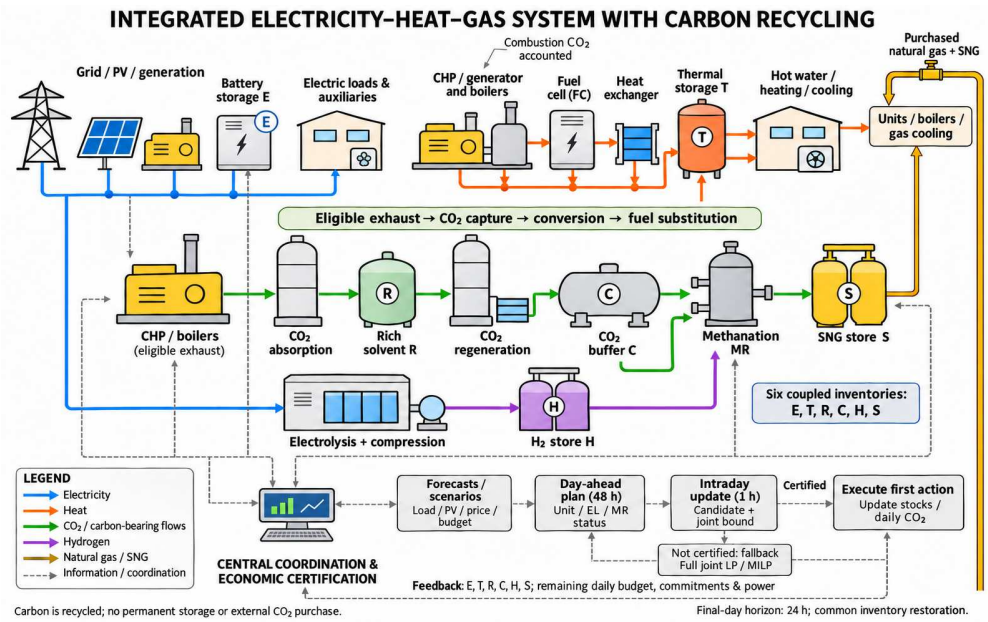

Fig. 1 Equipment configuration, carbon recycling, and dual-time-scale coordination in the electricity–heat–gas IES. CHP denotes an internal-combustion-engine combined heat and power unit; FC, fuel cell; EL, electrolyzer; and MR, methanation unit. CO_2 capture, regeneration, and methanation implement carbon recycling, coordinated through day-ahead scheduling and intraday updates. CO_2 emissions from synthetic natural gas (SNG) combustion are included in carbon accounting.

2.1 Energy and metering boundaries

The original measurements cover electricity, space heating, domestic hot water, cooling, photovoltaic (PV) generation, generator output, and equipment gas consumption. Historical equipment gas measurements are used for comparison; optimized gas purchases are determined by the fuel balance. The system retains the equipment scales of a 160-kW internal-combustion engine and a 200-kW fuel cell, and adds battery storage, thermal storage, carbon capture, an electrolyzer, a methanation unit, and associated buffer inventories. Section 4 distinguishes field data from additional engineering assumptions.

Flue gas eligible for capture originates from the engine and heating boilers; fuel-cell, gas-chiller, and regenerator exhaust is excluded. A dedicated gas-fired device supplies regeneration heat, and its fuel consumption, emissions, and operating expenditure are included in full. Recovered methanation heat enters the general heating bus;

low-grade waste heat is not assumed sufficient for solvent regeneration. The model includes neither external CO_2 purchases nor permanent storage, electricity exports, or gas exports. The ratings of the general heating and cooling plants are engineering expansion assumptions rather than a unit-by-unit reconstruction of all equipment at the original campus.

2.2 Dynamic carbon-inventory constraints and multienergy coupling

Let R, C, H, and S denote the CO_2 inventory in rich solvent, the regenerated-CO_2 buffer inventory, the hydrogen inventory, and the higher-heating-value (HHV) energy inventory of synthetic methane, respectively. Let E and T denote battery and thermal inventories. The mass flow rates q_{abs}, q_{reg}, and q_{MR} describe CO_2 absorption, regeneration, and methanation, while q_{H2} denotes hydrogen production. Fuel energy is measured on an HHV basis, and electrical and thermal energies are expressed in kWh with a time step $\Delta t = 1$ h. Inventories are defined at hourly boundaries, whereas flow rates and powers are hourly averages. Rich-solvent inventory is expressed as the equivalent mass of desorbable CO_2.

$$R(t) = R(t-1) + \Delta t\,[q_{\mathrm{abs}}(t) - q_{\mathrm{reg}}(t)] \tag{1}$$

$$C(t) = C(t-1) + \Delta t\,[q_{\mathrm{reg}}(t) - q_{\mathrm{MR}}(t)] \tag{2}$$

$$H(t) = H(t-1) + \Delta t\,[q_{\mathrm{H2}}(t) - (8/44)q_{\mathrm{MR}}(t)] \tag{3}$$

$$S(t) = S(t-1) + \Delta t\,[h_{\mathrm{CH4}}(16/44)q_{\mathrm{MR}}(t) - P_{\mathrm{SNG}}(t)] \tag{4}$$

$$E(t) = E(t-1) + \Delta t\,[\eta P_{\mathrm{ch}}(t) - P_{\mathrm{dis}}(t)/\eta] \tag{5}$$

Thermal inventory is updated by charging and discharging, using the same hourly discretization as the battery:

$$T(t) = T(t-1) + \Delta t\,[\eta_T Q_{\mathrm{ch}}(t) - Q_{\mathrm{dis}}(t)/\eta_T] \tag{6}$$

Here, Q_{ch} and Q_{dis} are the powers entering the thermal store and supplied from it to the heating bus, respectively, in kW. The one-way battery efficiency η and thermal-storage efficiency η_T are both 0.95; no separate standing-loss term is included. Battery and thermal inventories operate between 10% and 90% of rated capacity. Binary mode variables prevent simultaneous charging and discharging:

$$\begin{aligned}
&0.1E_{\max} \le E(t) \le 0.9E_{\max}, \quad 0.1T_{\max} \le T(t) \le 0.9T_{\max},\\
&0 \le P_{\mathrm{ch}}(t) \le P_{B,\max} z_B(t),\\
&0 \le P_{\mathrm{dis}}(t) \le P_{B,\max}[1 - z_B(t)],\\
&0 \le Q_{\mathrm{ch}}(t) \le Q_{T,\max} z_T(t),\\
&0 \le Q_{\mathrm{dis}}(t) \le Q_{T,\max}[1 - z_T(t)], \quad z_B(t), z_T(t) \in \{0,1\}.
\end{aligned} \tag{7}$$

In the main case, $E_{\max} = 400$ kWh and $T_{\max} = 800$ kWh; the charging/discharging power limits are $P_{B,\max} = 150$ kW and $Q_{T,\max} = 250$ kW. The four conversion inventories satisfy $0 \le R \le 200$ kg CO_2, $0 \le C \le 200$ kg CO_2, $0 \le H \le 25$ kg, and $0 \le S \le 1500$ kWh HHV. Together with Eqs. (1)–(6), these capacity bounds constrain intertemporal material and energy transfers.

Equations (1)–(4) connect absorption, regeneration, hydrogen production, methanation, and subsequent combustion into a continuous inventory chain. Rich-solvent storage decouples the timing of absorption and regeneration; the CO_2 and hydrogen buffers constrain methanation feedstock availability, while synthetic-methane storage connects conversion to subsequent fuel use. Battery and thermal storage jointly affect energy-supply timing for these processes. Economic MPC for capture (Chan and Chen 2018) and solvent-storage decoupling control (Qiu et al. 2025) provide related foundations. An inventory-level dynamic approximation is adopted here; process-model validation can draw on Weimann et al. (2023).

$$\begin{aligned} 0 \le q_{\text{abs}}(t) &\le 0.90 G_{\text{eligible}}(t), \\ 0 \le q_{\text{abs}}(t), q_{\text{reg}}(t) &\le 80 \text{ kg/h}. \end{aligned} \tag{8}$$

Full-load system electricity consumption of the electrolyzer is calibrated to 55 kWh/kg H_2, consistent with the DOE 2022 system-status reference (U.S. Department of Energy n.d.). A part-load approximation combines incremental consumption of 54 kWh/kg with an on-state idle demand of 9.09 kW; external hydrogen-storage compression requires an additional 1 kWh/kg. The technology classification and auxiliary-equipment boundary follow the water-electrolysis review in Buttler and Spliethoff (2018). Model applicability is discussed in Sect. 6.

$$\begin{aligned} P_{\text{EL}}(t) &= 54 q_{\text{H2}}(t) + 9.09 u_{\text{EL}}(t), \\ 50 u_{\text{EL}}(t) \le P_{\text{EL}}(t) &\le 500 u_{\text{EL}}(t). \end{aligned} \tag{9}$$

The minimum stable methanation load is 45%. A 130-s hot-start time is represented as a reduction in hourly-average output, following a specific reactor study (Giglio et al. 2021); operating windows also vary with equipment design (Herrmann et al. 2022). This parameter represents hot-standby operation only and does not resolve cold-start temperatures or continuous heat-maintenance power. Electrolyzer/methanation startup energies of 2/5 kWh are common engineering assumptions.

$$q_{\text{MR}}(t) \le 45[u_{\text{MR}}(t) - (130/3600) v_{\text{start,MR}}(t)] \tag{10}$$

$$q_{\text{MR}}(t) \ge 0.45 \times 45[u_{\text{MR}}(t) - (130/3600) v_{\text{start,MR}}(t)] \tag{11}$$

The generators retain output bounds, a part-load fuel approximation, minimum up/down times, and ramping constraints, with the previous 24 h of operating history carried across days. For $j \in \{\text{CHP}, \text{FC}\}$, V_j is the gas volume flow rate (m^3/h), P_j and Q_j are electrical output and utilized recovered-heat power, and u_j is the on/off status. Fuel use and heat recovery are coupled as follows:

$$
\begin{aligned}
V_j(t) &= r_j[0.1P_{j,\max}u_j(t) + 0.9P_j(t)],\\
0.4P_{j,\max}u_j(t) \le P_j(t) &\le P_{j,\max}u_j(t),\\
0 \le Q_j(t) &\le \kappa_j P_j(t), \quad j \in \{\mathrm{CHP}, \mathrm{FC}\}.
\end{aligned}
\tag{12}
$$

The ratings are $P_{\mathrm{CHP},\max} = 160$ kW and $P_{\mathrm{FC},\max} = 200$ kW. Fuel coefficients $r_{\mathrm{CHP}} = 0.299375$ m^3/kWh and $r_{\mathrm{FC}} = 0.2630927835$ m^3/kWh are calibrated from 2003 measurements. Heat-recovery coefficients are $\kappa_{\mathrm{CHP}} = 1.662020906$ and $\kappa_{\mathrm{FC}} = 0.5$. Recovered heat is utilized according to demand rather than forced to its upper bound. Both the minimum up and down times are 1 h for the CHP and 4 h for the FC. Normal-operation ramp limits are 160 and 50 kW/h, respectively; startup, shutdown, and historical states enter the boundary-hour constraints.

Let Q_{HP} and Q_{DHW} denote the heating-plant and domestic-hot-water-boiler outputs. Recovered methanation heat Q_{MR}, dedicated-regenerator fuel-energy flow F_{reg}, and the eligible flue-gas CO_2 source G_{eligible} are

$$
\begin{aligned}
Q_{\mathrm{MR}}(t) &= 0.70 \times 1.041666667 q_{\mathrm{MR}}(t)\\
&= 0.729166667 q_{\mathrm{MR}}(t),\\
F_{\mathrm{reg}}(t) &= h_{\mathrm{reg}} q_{\mathrm{reg}}(t)/\eta_{\mathrm{reg}},\\
G_{\mathrm{eligible}}(t) &= e_{\mathrm{gas}}[h_{\mathrm{gas}} V_{\mathrm{CHP}}(t)\\
&\qquad + Q_{\mathrm{HP}}(t)/\eta_{\mathrm{HP}} + Q_{\mathrm{DHW}}(t)/\eta_{\mathrm{DHW}}].
\end{aligned}
\tag{13}
$$

Here, $h_{\mathrm{reg}} = 1$ kWh/kg CO_2, $\eta_{\mathrm{reg}} = 0.90$, $\eta_{\mathrm{HP}} = 0.93$, $\eta_{\mathrm{DHW}} = 0.90$, and $h_{\mathrm{gas}} = 12.5$ kWh HHV/m^3. The source G_{eligible}, in kg CO_2/h, includes only engine, heating-plant, and domestic-hot-water-boiler exhaust; FC, cooling, and regenerator exhaust is excluded. Regeneration heat is supplied by the dedicated gas-fired device associated with F_{reg} and is not counted again as demand on the general heating bus.

The electricity-bus balance and carbon-recycling-device electricity demand are

$$
\begin{aligned}
P_{\mathrm{grid}} + P_{\mathrm{PV}} + P_{\mathrm{CHP}} + P_{\mathrm{FC}} + P_{\mathrm{dis}} &= L_e + P_{\mathrm{ch}} + P_{\mathrm{cycle}},\\
P_{\mathrm{cycle}} &= P_{\mathrm{EL}} + P_{\mathrm{comp}} + P_{\mathrm{aux}} + P_{\mathrm{start}},\\
P_{\mathrm{comp}} &= 1.0 q_{\mathrm{H2}},\\
P_{\mathrm{aux}} &= 0.10 q_{\mathrm{abs}} + 0.05 q_{\mathrm{reg}},\\
P_{\mathrm{start}} &= [2v_{\mathrm{start,EL}} + 5v_{\mathrm{start,MR}}]/\Delta t.
\end{aligned}
\tag{14}
$$

The common time index t is omitted in Eqs. (14)–(17). Here, L_e is the base electrical load and P_{PV} is utilized PV output, satisfying $0 \le P_{\mathrm{PV}} \le P_{\mathrm{PV,avail}}$. PV curtailment is permitted, but electricity exports are not. Electricity coefficients for compression, absorption, and regeneration auxiliaries are 1.0 kWh/kg H_2, 0.10 kWh/kg CO_2, and 0.05 kWh/kg CO_2, respectively. Startup indicators $v_{\mathrm{start,EL}}$ and $v_{\mathrm{start,MR}}$ convert startup energies of 2 and 5 kWh into power through division by Δt.

Heating and cooling are coupled through the thermal input $Q_{\mathrm{AC,in}}$ to the recovered-heat chiller. The heating and cooling buses satisfy

$$
\begin{aligned}
Q_{\mathrm{CHP}} + Q_{\mathrm{FC}} + Q_{\mathrm{HP}} + Q_{\mathrm{DHW}} + Q_{\mathrm{MR}} + Q_{\mathrm{dis}}\\
= L_{\mathrm{space}} + L_{\mathrm{DHW}} + Q_{\mathrm{ch}} + Q_{\mathrm{AC,in}} + Q_{\mathrm{spill}}.
\end{aligned}
\tag{15}
$$

$$Q_{\mathrm{GC}} + \mathrm{COP}_{\mathrm{AC}} Q_{\mathrm{AC,in}} = L_c + Q_{c,\mathrm{spill}}, \quad \mathrm{COP}_{\mathrm{AC}} = 0.70 \tag{16}$$

The loads L_{space}, L_{DHW}, and L_c represent space heating, domestic hot water, and cooling. The gas chiller supplies cooling power Q_{GC}, while $Q_{\mathrm{AC,in}}$ is the heat consumed by the recovered-heat chiller. The gas chiller has an HHV-based $\mathrm{COP}_{\mathrm{GC}} = 1.10$. Heat and cooling rejection, Q_{spill} and $Q_{c,\mathrm{spill}}$, are limited to 500 and 250 kW, with the disposal tariff specified in Table 3. The limits on Q_{HP}, Q_{DHW}, and Q_{GC} are 5000, 80, and 5000 kW; the limit on $Q_{\mathrm{AC,in}}$ is 5000/0.70 kW.

Total fuel demand includes all generators, boilers, cooling equipment, and the dedicated regenerator:

$$\begin{aligned} F_{\mathrm{total}} = {} & h_{\mathrm{gas}}(V_{\mathrm{CHP}} + V_{\mathrm{FC}}) + Q_{\mathrm{HP}}/\eta_{\mathrm{HP}} \\ & + Q_{\mathrm{DHW}}/\eta_{\mathrm{DHW}} + Q_{\mathrm{GC}}/\mathrm{COP}_{\mathrm{GC}} + F_{\mathrm{reg}}. \end{aligned} \tag{17}$$

The fuel-energy flow F_{total}, in kW HHV, includes purchased natural gas and SNG combustion. Grid and gas imports are limited to 2500 kW and 2000 m^3/h, and SNG use to 500 kW HHV. Fuel-supply balance and emissions accounting are given in Sect. 2.3. These relationships and the device inventories define a unified electricity–heat–cooling–gas supply–demand boundary.

2.3 Operational emissions accounting and inventory closure

$$e(t) = \xi_{\mathrm{grid}} P_{\mathrm{grid}}(t) + e_{\mathrm{gas}} F_{\mathrm{total}}(t) - q_{\mathrm{abs}}(t) \tag{18}$$

$$h_{\mathrm{gas}} V_{\mathrm{buy}}(t) + P_{\mathrm{SNG}}(t) = F_{\mathrm{total}}(t) \tag{19}$$

$$\begin{aligned} \sum \Delta t \, [e_{\mathrm{gas}} F_{\mathrm{total}} - q_{\mathrm{abs}}] = {} & e_{\mathrm{gas}} \sum \Delta t \, h_{\mathrm{gas}} V_{\mathrm{buy}} \\ & - \Delta[R + C + e_{\mathrm{gas}} S]. \end{aligned} \tag{20}$$

The total fuel flow includes SNG combustion and regenerator fuel. When the relevant initial and final inventories are equal, net on-site emissions equal the CO_2 associated with purchased fossil gas; indirect grid emissions are accounted for separately. Carbon consumed in methanation is not credited as permanent sequestration (International Energy Agency 2019). Conversion and substitution use a common boundary (Götz et al. 2016; Schiebahn et al. 2015). Unlike the life-cycle environmental assessment of energy-storage pathways in Sternberg and Bardow (2015), the present study evaluates only operational emissions and does not perform a life-cycle assessment.

Each validation window spans three consecutive days. All six inventories, generator outputs, and the previous 24 h of commitment history carry across days. Define the inventory vector in the order $x = (E, T, R, C, H, S)$, with d indexing the operating day within a window. The common initial target x^* sets battery and thermal stores to 50% of rated capacity and the other four inventories to zero. Thus, in the main case, $E^* = 200$ kWh, $T^* = 400$ kWh, $R^* = C^* = 0$ kg CO_2, $H^* = 0$ kg, and $S^* = 0$ kWh HHV. Inventories are not reinitialized on intermediate days, and the same target is restored at the window endpoint $K = 72$ h:

$$\begin{aligned} x_d(0) &= x_{d-1}(24), \quad d = 2, 3, \\ x(0) &= x(K) = x^*, \quad K = 72. \end{aligned} \tag{21}$$

Nonfinal days use 48-h predictions and normalized terminal deviations to encourage inventory restoration. The final day uses a 24-h horizon and imposes Eq. (21) as a hard constraint. For scenario s and prediction endpoint N, the nonfinal-day soft terminal term is

$$\begin{aligned} x_{i,s}(N) - x_i^* &= \delta_{i,s}^+ - \delta_{i,s}^-, \quad i = 1, \ldots, 6, \\ D_{\text{stock},s} &= \sum_{i=1}^{6} \frac{\delta_{i,s}^+ + \delta_{i,s}^-}{X_{i,\max}}, \\ 0 &\le \delta_{i,s}^+, \delta_{i,s}^- \le X_{i,\max}. \end{aligned} \tag{22}$$

Here, $X_{i,\max}$ is the rated capacity of inventory i. Capacity changes update x^*, physical bounds, and normalization scales together, maintaining a consistent restoration convention in parameter sweeps. Intraday cumulative emissions are the sum of realized hourly emission rates multiplied by Δt, reset to zero each day and compared with that day's budget. Inventories remain continuous across days. Figure 4 shows the representative day, and Fig. 5 shows its complete three-day window and terminal restoration.

3 Dual-Time-Scale Coordination of Carbon Inventories and Daily Carbon Budgets

3.1 Day-ahead scheduling and daily-budget propagation

Day-ahead scheduling forms a 48-h plan using the information then available. Intraday forecasts are updated hourly, executed actions are fixed, and subsequent dispatch is constrained by current inventories and realized emissions. Both strategies fix the current day's commitment to their own day-ahead schedule and replan on the next day from the carried operating state. Equipment and adjustment permissions are identical; inventories and subsequent day-ahead schedules evolve with each method's feedback.

$$\begin{aligned} J_{\text{run}} = \sum \Delta t \, [&p_e(t) P_{\text{grid}}(t) + p_g V_{\text{buy}}(t) \\ &+ c_{\text{OM}}(t) + \lambda_C e(t)] + \sum c_{\text{start}} v_{\text{start}}. \end{aligned} \tag{23}$$

$$\sum_{t \in \text{day}} \Delta t \, e(t) \le B_{\text{day}} + \varepsilon_{\text{day}}, \quad \varepsilon_{\text{day}} \ge 0 \tag{24}$$

Operating expenditure comprises energy purchases, operation and maintenance (O&M), startup, storage throughput, and energy-disposal costs. The operating objective J_{run} additionally includes a carbon shadow cost of 0.21212 CNY/kg. The online predictive objective also includes a budget-slack penalty of 21.212 CNY/kg and normalized terminal-inventory terms, as defined in Sect. 3.2. Monetary values, objectives, and economic bounds are expressed in CNY using the exchange-rate convention in Sect. 4.2.

$$B_{\mathrm{day}} = 0.95E_{\mathrm{proxy}}(\mathrm{DAforecast}) + \max[0, Q_{0.75,\mathrm{month}}(\mathrm{error}_{2004})] \tag{25}$$

The emissions proxy E_{proxy} uses historical forecasts and a fixed reference operating relationship. Development-period residuals are the actual proxy minus 0.95 times the forecast proxy; monthly 75th percentiles are fixed using 2004 data. Test-day budgets use only information available at the time. Intraday optimization fixes emissions from executed periods and sets the remaining allowance to the daily budget minus realized emissions, together with the slack in Eq. (24). Thus, a fresh full-day allowance is not granted at every update. Budgets are accounted for daily, while inventories carry across days; related concepts of committed carbon-emission operating regions for IESs are presented in Jiang et al. (2024).

3.2 Multiscenario receding-horizon coordination and economic-quality certification

The scenario set contains a nominal forecast and three seasonal error scenarios, with empirical weights w_s. Scenarios share the current-period action and inventory state, allow scenario-specific compensation in later periods, and use common budget slack ε_d for a given day. This two-stage receding-horizon approximation jointly considers remaining emissions allowances, subsequent conversion energy demand, and inventory restoration. Its objective includes the operating objective, a 21.212-CNY/kg budget-slack penalty, and normalized terminal deviations on nonfinal days. The terminal-deviation coefficient is 4.2424 CNY; final-day inventory restoration is enforced as a hard constraint.

$$J_{\mathrm{pred}} = \sum_{s\in\mathcal{S}} w_s J_{\mathrm{run},s} + \rho_B \sum_{d\in\mathcal{D}} \varepsilon_d + \rho_T \sum_{s\in\mathcal{S}} w_s D_{\mathrm{stock},s} \tag{26}$$

The maximum budget slack required by the scenario candidates is used as common slack. Variable bounds, physical constraints, integrality, and the common first action are checked against the original joint matrix to obtain a feasible objective upper bound U.

$$\varepsilon_d = \max_{s\in\mathcal{S}} \varepsilon_{s,d}, \qquad U = \sum_{s\in\mathcal{S}} w_s J_s(z_s, \varepsilon) \tag{27}$$

Write the joint constraints as $l \le Ax \le u$ and $a \le x \le b$. Only integrality is relaxed; the shared current actions and budget constraints are retained. For row multipliers y, Eq. (28) constructs a compensated Lagrangian lower bound. Multipliers selecting infinite row endpoints are set to zero, and variable bounds compensate the residual $c - A^{\mathsf{T}}y$. The bound is recomputed using the current right-hand sides and variable bounds; cached information is invalidated whenever A or c changes.

$$L(y) = \min_{l\le z\le u} y^{\mathsf{T}} z + \min_{a\le x\le b} (c - A^{\mathsf{T}}y)^{\mathsf{T}} x \tag{28}$$

Proof: for any feasible x, $c^{\mathsf{T}}x = y^{\mathsf{T}}Ax + (c - A^{\mathsf{T}}y)^{\mathsf{T}}x$. Each term is no smaller than its minimum over the corresponding bounds, hence $L(y) \le J^*$. The optimum of the joint linear-programming (LP) relaxation retaining coupling constraints is no lower

than the optimum of independent LP relaxations. However, a bound constructed from cached multipliers need not exceed a freshly solved independent-LP lower bound.

After subtracting the objective constant C_{past} associated with executed actions, the absolute tolerance is 0.042424 CNY and the relative tolerance remains 0.1%. A candidate is accepted only if it is fully feasible and satisfies Eq. (29). Since $L \leq J^* \leq U$, its current finite-horizon objective error satisfies $U - J^* \leq U - L$.

$$U - L \leq 0.042424 + 0.001 \max\{0.042424, |U - C_{\text{past}}|\} \tag{29}$$

Equation (29) bounds the candidate objective error for the current finite-scenario optimization problem. Closed-loop performance and stability in economic MPC require additional dissipativity, terminal, and feasible-set conditions (Angeli et al. 2012; Mayne et al. 2000). The interpretation is delimited in Sect. 6.

3.3 Inventory-trajectory reuse and fallback optimization

Executed actions and inventories are updated at each step. Previously saved scenario trajectories serve as candidate templates. The nominal trajectory generates a common current action, while subsequent device-control sequences are retained as far as possible within each scenario. When current flows change, the six inventories are propagated using the conservation relationships in Sect. 2, and nonfinal-day terminal-deviation variables are updated. Candidates violating capacity, commitment, ramping, carbon-source, or terminal constraints are rejected. Final-day candidates must still satisfy hard inventory restoration.

Under updated forecasts, external energy supply is adjusted through electricity purchases, heating, cooling, and gas purchases, after which emissions and shared daily-budget slack are recalculated. If trajectory stitching fails, the complete device-control sequence of the same template is tried. The same template generates the current action across scenarios, and identical current load and PV observations are used. Every candidate is ultimately checked against the original joint matrix.

Failure to obtain certification triggers a full joint LP/MILP solve. After two consecutive cached-candidate failures, candidate construction is skipped for the next two hours. Candidate checks, fallback solves, and model updates are all included in computation time.

Full joint optimization and the proposed method share an idle-storage mode reconstruction rule. If first-step charging and discharging powers are numerically zero, an integer mode satisfying common rules and historical states is selected. LP integer reconstruction is accepted only after checking the original matrix and objective; otherwise, the MILP is solved.

3.4 Comparison strategies and common settings

Table 1 summarizes the two comparison strategies. The methods use identical site inputs, predictors, device capacities, carbon budgets, solution tolerances, day-ahead planning, and commitment-adjustment rules. Both transfer inventories correctly and accumulate realized emissions. Conventional MPC uses the nominal forecast, whereas

Table 1 Comparison strategies and common equipment permissions.

Method	Forecasting and solution	Common equipment permissions
Conventional MPC	Nominal forecast; full solve every hour	Current-day commitment fixed to its day-ahead schedule
Proposed method	Four forecast scenarios; inventory-trajectory candidates and a joint economic certificate; full solve if certification fails	Current-day commitment fixed to its day-ahead schedule

the proposed method constructs four empirical scenarios from the same available information without additional future observations. The comparison therefore evaluates the combined effects of scenario treatment and trajectory reuse.

4 Data, Parameters, and Validation Protocol

4.1 Public field data and engineering retrofit

Hourly campus data published by Liao et al. (2024b) are used. The columns "Heating load (kW)" and "Hot water load (kW)" in the prepared Figshare archive 43992003 are mapped to space-heating and domestic-hot-water power with input multipliers of one. The code `carbon_v4_study.py` assigns the columns directly, without further MJ-to-kWh conversion or scaling. Hourly heat is calculated as $Q = P\Delta t$, with $\Delta t = 1$ h; its value in kWh therefore equals the hourly-average power in kW. Table 2 summarizes these conventions.

Table 2 Thermal-load input units and time-integration conventions.

Data item	Source unit	Input or integration rule	Model unit
Prepared space-heating column	kW	Direct input; multiplier 1	kW
Prepared hot-water column	kW	Direct input; multiplier 1	kW
Hourly thermal energy	Power in kW	$Q = P\Delta t$, $\Delta t = 1$ h	kWh

Across 35,064 hourly records from 2003, 2004, 2009, and 2010, the prepared heating and hot-water columns have fixed ratios of 63.7934 and 0.2778, respectively, to the corresponding Raw Data columns, with zero maximum mapping residual. Both file sets are labeled kW, and the public script does not explain the underlying physical calibration of these ratios; the prepared-data power convention is adopted. The original

preprocessing includes median imputation without pointwise flags, and no additional imputation is performed here. Equipment gas data provide historical comparisons; added equipment is modeled as an engineering retrofit scenario.

The day-ahead forecast is 0.7 times the hourly median of the preceding four corresponding weekdays plus 0.3 times the last completed day's profile. Forecasting the following day likewise excludes any unobserved part of the current day's complete profile. Intraday updates use only the latest observed errors and autoregressive decay estimated from 2003 data. A dedicated causality test verified that perturbing future realized loads does not change current forecasts or budgets. Energy-carrier errors are normalized by their 2003 95th percentiles rather than by near-zero mean heat loads.

PV generation retains the hourly shape of the original 153-kW installation. The main case applies a common capacity multiplier of 20, representing an approximately 3.06-MW expansion; the original multiplier of one is also evaluated in sensitivity analysis. This common engineering assumption represents a high-renewable-output case rather than an actual campus expansion.

4.2 Parameter boundaries and inventory consistency

Table 3 lists the main reference-case parameters. Electricity tariffs (Kyushu Electric Power n.d.), gas prices (Saibu Gas n.d.), and the grid emissions factor (Kyushu Electric Power 2025) are public references from years different from the load records. The selected gas price is the FY2016 pretax reference of 58.4 JPY/m^3 for annual consumption of at least 10^6 m^3, at 45 MJ/m^3; its converted value is 2.4776 CNY/m^3. This tier is a price scenario, not an inferred campus contract. The electricity scenario uses the earlier schedule labeled "through October 31" in Kyushu Electric Power (n.d.): peak, summer-day, other-day, and night prices are 29.25, 25.15, 24.12, and 15.17 JPY/kWh, respectively, including tax. Dividing by 1.10 before currency conversion gives the pretax range 0.5851–1.1281 CNY/kWh. Demand charges and fuel-price adjustments are excluded. The experimental time-of-use mapping treats Sundays as all-night-rate days and omits the supplier's additional holiday calendar. The provisional FY2024 unadjusted annual grid factor reported in the FY2025 plan is 0.31 kg CO_2/kWh; the same source gives basic and adjusted factors of 0.449, which is tested separately. These values define a common engineering scenario for comparing operating expenditure.

All monetary quantities are expressed in CNY. Using the official central parity rate on November 2, 2026, 100 JPY equals 4.2424 CNY, or 1 JPY equals 0.042424 CNY. Amounts, prices, penalties, objective bounds, and absolute tolerances from the original solver archive are multiplied by the same factor for presentation. Relative changes, statistical tests, physical dispatch, and timing remain unchanged; the optimization was not rerun for currency conversion. The exchange-rate source is the November 2, 2026 record in the State Administration of Foreign Exchange central parity database (State Administration of Foreign Exchange 2026).

A common capacity mapping updates initial states, physical bounds, terminal targets, and normalized penalties for all six inventories. Capacity multipliers do not alter efficiencies or operating-cost coefficients. On the hourly grid, EL/MR ramp limits equal their rated capacities; inventory evolution, generator minimum up/down times, and regenerator ramping provide the principal dynamic restrictions.

Table 3 Main equipment and reference-case parameters.

Parameter	Value	Basis or qualification
Generator ratings	160 / 200 kW	Published ratings; fuel calibrated on 2003 data.
Battery / thermal storage	400 / 800 kWh	One-way efficiency 0.95.
Rich-solvent CO_2 / buffered CO_2 / H_2	200 / 200 / 25 kg	CO_2 mass for rich solvent/buffer; H_2 mass for hydrogen.
SNG storage / use	1500 kWh HHV / 500 kW HHV	Consistent HHV gas-energy basis.
EL rating / system consumption	500 kW / 55 kWh/kg H_2	DOE status reference; part-load curve is a proxy.
MR rating / minimum load	45 kg CO_2/h / 45%	Assumed capacity; load range follows a specific reactor (Giglio et al. 2021).
Absorption / regeneration limits	80 / 80 kg CO_2/h	Regeneration ramp: 40 (kg CO_2/h)/h.
Absorption / regeneration auxiliaries	0.10 / 0.05 kWh/kg CO_2	Steady-state total: 0.15 kWh/kg CO_2.
Regeneration heat / efficiency	1 kWh/kg CO_2 / 0.90	Heat boundary: Sect. 6.
Grid emissions factor	0.31 kg CO_2/kWh	Provisional FY2024 annual (Kyushu Electric Power 2025); unadjusted, not marginal.
Gas price / heating value	2.4776 CNY/m^3 / 45 MJ/m^3	Public FY2016 reference (Saibu Gas n.d.); not the campus contract price.
Time-of-use electricity price	0.5851–1.1281 CNY/kWh	Earlier pretax schedule (Kyushu Electric Power n.d.); no demand charges or adjustments.
Rejection tariff	0.0021212 CNY/kWh	Same for heat and cooling.

Note: Storage capacities and added-device values are engineering assumptions except where a specific source or calibration is identified.

4.3 Parameter screening and cross-year multiday validation

The 2003 data train the predictor and calibrate fuel relationships; the 2004 data calibrate budgets and screen parameters. One or four candidate templates and relative tolerances of 0.1%, 0.2%, or 0.5% define six configurations. Eight common-input days are replayed under identical day-ahead schedules, using full scenario MPC as the reference. Configurations with an operating-expenditure increase no greater than 0.2% and a total budget-exceedance increase no greater than 1 kg qualify for comparison; selection then uses intraday online computation time.

Before cross-year validation, parameters are fixed to one candidate template, a 0.1% relative tolerance, and a two-hour pause after two consecutive candidate failures. Tests use 2009 and 2010: a three-day window begins on the first Monday on or after

the tenth of each month, giving 24 windows and 72 operating days. Previous-day inventories and operating history carry within each window to test interday effects. The 24 windows are the paired statistical units; the two strategies produce 144 daily trajectories. Dates are calendar-prespecified, and model or algorithm parameters are not adjusted according to test outcomes.

Matrices, executed prefixes, and numerical handling for solver exceptions are retained in the reproducibility archive. Inconsistent warm-start statuses are checked by cold-starting the same matrix before execution resumes; original failures and timing provenance are retained.

4.4 Metrics and statistical criteria

Operating expenditure, operational CO_2 emissions, budget exceedance, compliance days, inventory errors, and end-to-end computation time are reported separately. Operating expenditure excludes carbon shadow costs and budget-control penalties. End-to-end time includes day-ahead seeds, model construction, loading, forecast updates, candidates, bound evaluation, failures, and fallback solves, but excludes file writing and ex post auditing. Both methods use identical solution tolerances and eligibility for numerical handling.

$$E_{\text{excess}} = \max(0, E_{\text{actual}} - B), \quad J_{\text{eval}} = J_{\text{run}} + 21.212 E_{\text{excess}} \tag{30}$$

Using the 24 three-day windows as paired units, 20,000 bootstrap resamples with seed 20261101 yield 95% confidence intervals; two-sided Wilcoxon test results are also reported. Comparison with conventional MPC is a secondary analysis under the prespecified protocol and is interpreted as exploratory, without multiplicity correction for secondary outcomes.

Dolan and Moré (2002) introduced performance profiles for solver benchmarking. Here, paired-window statistics are accompanied by the worst deterioration, the fraction of favorable windows, and all computational failures. Interval estimates apply to the two tested years, and months need not be mutually independent. The four empirical scenarios also differ from independent and identically distributed samples in convex stochastic programming; generic confidence guarantees from the scenario approach are therefore not invoked (Schildbach et al. 2014; Campi and Garatti 2008).

5 Multi-Day Validation Results and Operating Conditions

5.1 Operating expenditure, emissions, and carbon-budget compliance

Table 4 summarizes the aggregate results. Across the 72 operating days in 24 prespecified windows, the proposed method saves 8324.58 CNY relative to conventional MPC, approximately 0.81%, and reduces operational CO_2 emissions by approximately 4.73 t, or 0.84%. Total budget exceedance decreases by approximately 618 kg; both methods satisfy their daily budgets on 57 days. Expenditure changes are recomputed

Table 4 Operating expenditure, emissions, compliance, and computation time over 72 days.

Method	Expenditure (10^4 CNY)	Operational CO_2 (t)	Exceedance (kg)	Compliant days	End-to-end time (s)
Conventional MPC	103.319	562.71	15404.7	57/72	163.4
Proposed method	102.487	557.99	14786.4	57/72	188.0

Note: Monetary values are in CNY. Totals are rounded for display; differences, percentages, and intervals use consistently converted unrounded values.

from executed energy purchases, O&M, and other cash-cost components; reductions in control penalties are not counted as cash savings.

The 95% paired interval for expenditure savings is [1373.55, 16118.82] CNY, with an exploratory two-sided $p = 0.039$. The 95% interval for the emissions difference is $[-7.41, -2.40]$ t. The budget-exceedance difference has a 95% interval of $[-2747, 1217]$ kg, which spans zero. End-to-end computation time increases from 163.4 to 188.0 s, a difference of approximately 24.6 s or 15.1%; the 95% interval for the time difference is [10.5, 38.7] s.

5.2 Window-to-window differences and independent verification

Operating expenditure decreases in 16 of the 24 prespecified windows and increases in eight, with a maximum increase of approximately 2.22%. End-to-end computation is faster in six windows, and the maximum time ratio is approximately 2.38. Figure 2 presents all windows. Of 1728 online updates, 108 candidate schedules pass economic-quality certification, corresponding to 6.25%.

For every certified candidate, an independent program checks constraint feasibility against the original matrix and recomputes its objective upper bound and compensated lower bound, verifying finite-horizon predictive objective quality.

Independent replay covers 216 archived trajectories and 5184 executed steps; the two strategies reported here account for 144 trajectories and 3456 steps. All 108 accepted certificates are also verified, with 28 reference solves selected by a prespecified rule. The maximum original-matrix residual is approximately 8.4×10^{-8}, expenditure-recomputation error is below 9×10^{-11} CNY, interday states are consistent, and the terminal residual is below 5×10^{-11}.

5.3 Representative-day dispatch and carbon-inventory evolution

Representative days are prespecified as the second days of the winter, spring, summer, and autumn windows in 2009: January 13, April 14, July 14, and October 13. Figure 3 shows electricity–heat–gas dispatch on April 14; Fig. 4 gives the corresponding six

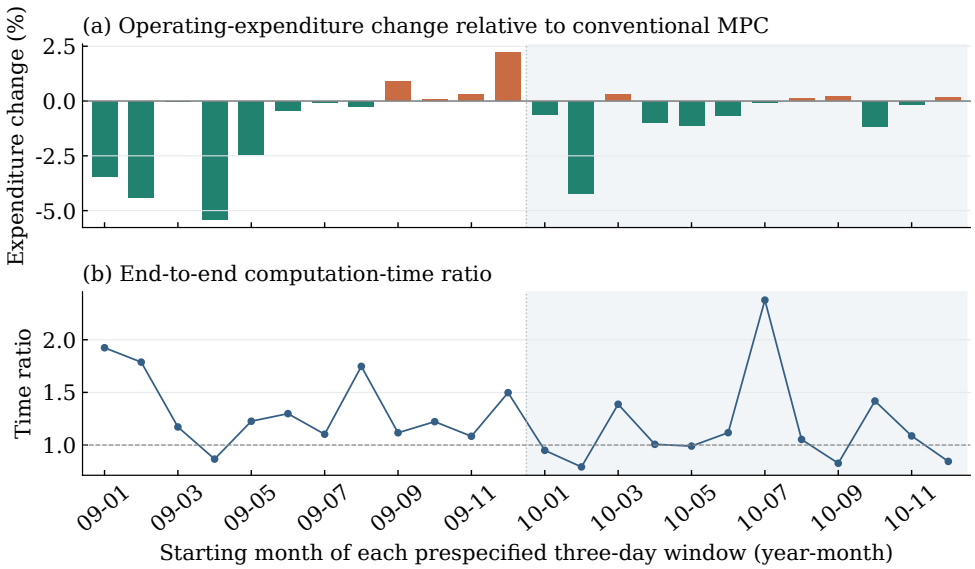

Fig. 2 Proposed method relative to conventional MPC over all 24 three-day windows. Operating-expenditure changes use conventional MPC as the denominator; end-to-end computation-time ratios divide proposed-method time by conventional-MPC time. The vertical dotted line separates 2009 and 2010.

inventories and cumulative emissions. Figure 5 extends the view to the full April 13–15 window. Both inventory figures use hourly numerical values from the frozen results without smoothing, interpolation, or manual adjustment.

Figures 3 and 4 jointly show supply dispatch and inventory evolution. Thermal storage discharges during 00:00–05:00, charges during 05:00–07:00, and then discharges until approximately 11:00. The proposed method replenishes thermal inventory to approximately 720 kWh during 15:00–22:00. During 12:00–13:00, the electrolyzer remains at 50 kW and grid imports are approximately 125 kW; during 13:00–14:00, electrolyzer power rises to 500 kW and imports increase to approximately 1348 kW, illustrating that hydrogen-production load shifting remains constrained by contemporaneous supply and demand. During 11:00–15:00, regeneration consumes rich solvent carried from the previous day, while methanation uses buffered CO_2 and hydrogen. Rich-solvent carbon inventory falls from approximately 124 to 63 kg, and the resulting SNG is subsequently combusted. On this day, proposed-method cumulative emissions exceed those of conventional MPC, and both methods exceed the common daily budget. Interday differences are evaluated using the complete three-day window and the aggregate statistics in Sect. 5.1.

The representative day is the middle day of a three-day window, so its final inventory need not equal its own initial inventory. Figure 5 shows that both methods carry preceding-day states at 24 and 48 h and restore battery and thermal inventories to 200 and 400 kWh at 72 h, with rich-solvent, CO_2-buffer, hydrogen, and SNG inventories returning to zero. Intermediate inventory withdrawals and subsequent restoration

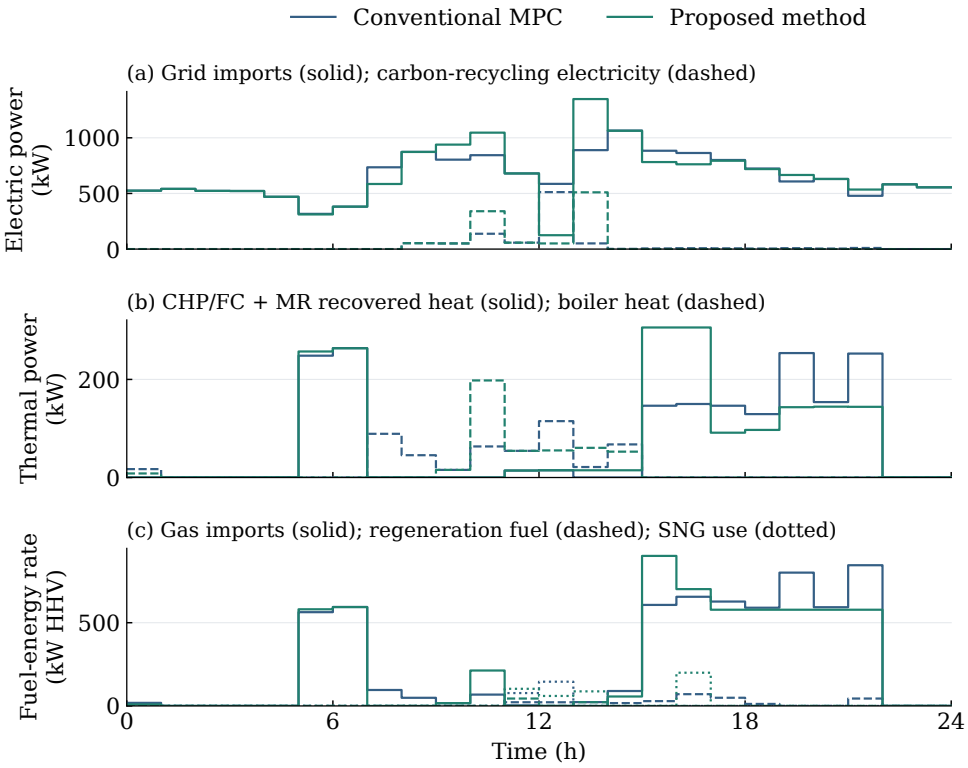

Fig. 3 Key electricity, heat, and gas dispatch of conventional MPC and the proposed method on the prespecified spring representative day. Colors distinguish methods, and line styles distinguish energy flows. Carbon-recycling electricity demand includes electrolysis, compression, capture/regeneration auxiliaries, and startup energy.

enter the same evaluation, preventing temporary depletion of unrestored inventories from being counted as a cycle benefit.

Rechecking all 24 windows confirms zero interday inventory-transfer error over the two methods' 144 daily trajectories and 3456 executed steps. The maximum terminal numerical deviation normalized by rated capacity is below 3×10^{-13}. Daily budgets and emissions in the figure come from the same archived solves. Inventory closure and daily compliance are checked separately, and multiday performance uses the common statistics in Sect. 5.1.

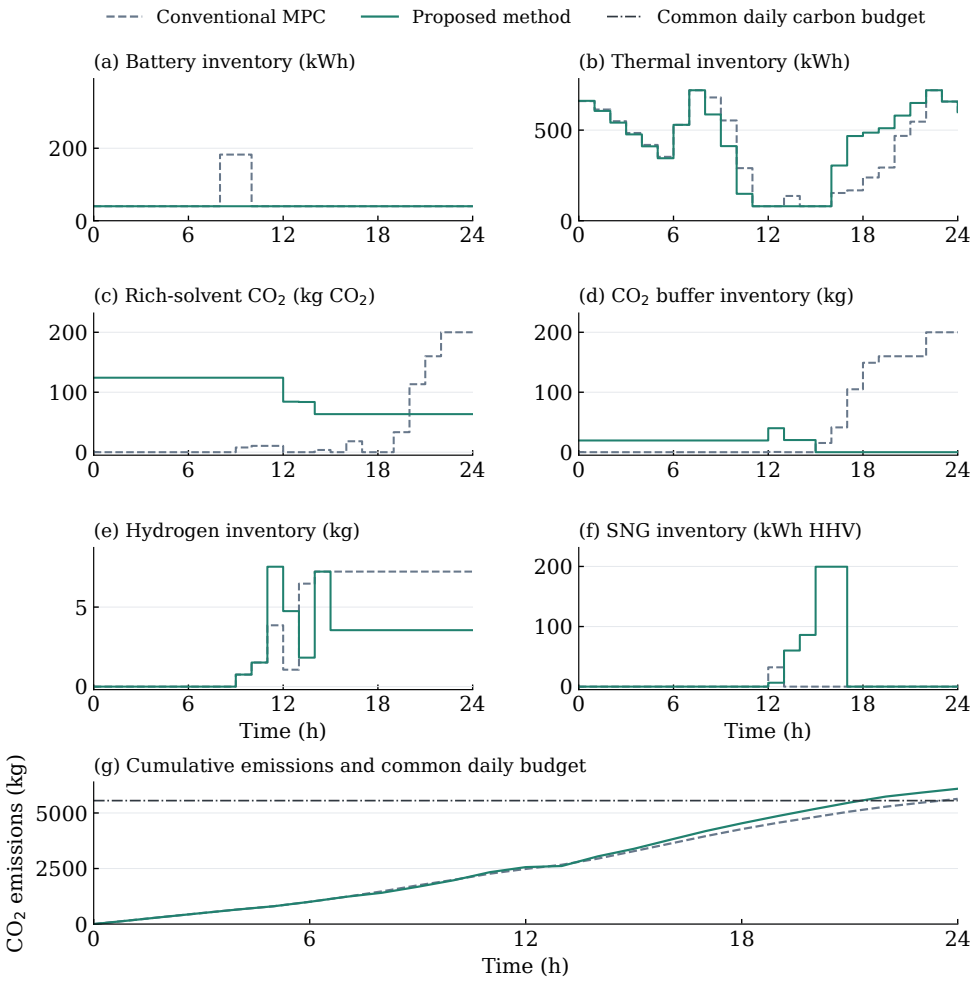

Fig. 4 Six inventories and cumulative emissions on the prespecified representative day, April 14, 2009. Curves are taken directly from original hourly optimization trajectories. Dashed lines denote conventional MPC, solid lines the proposed method, and the dash-dotted line the common daily carbon budget. Inventories are shown at hourly boundaries; each method's initial state carries over from the preceding day.

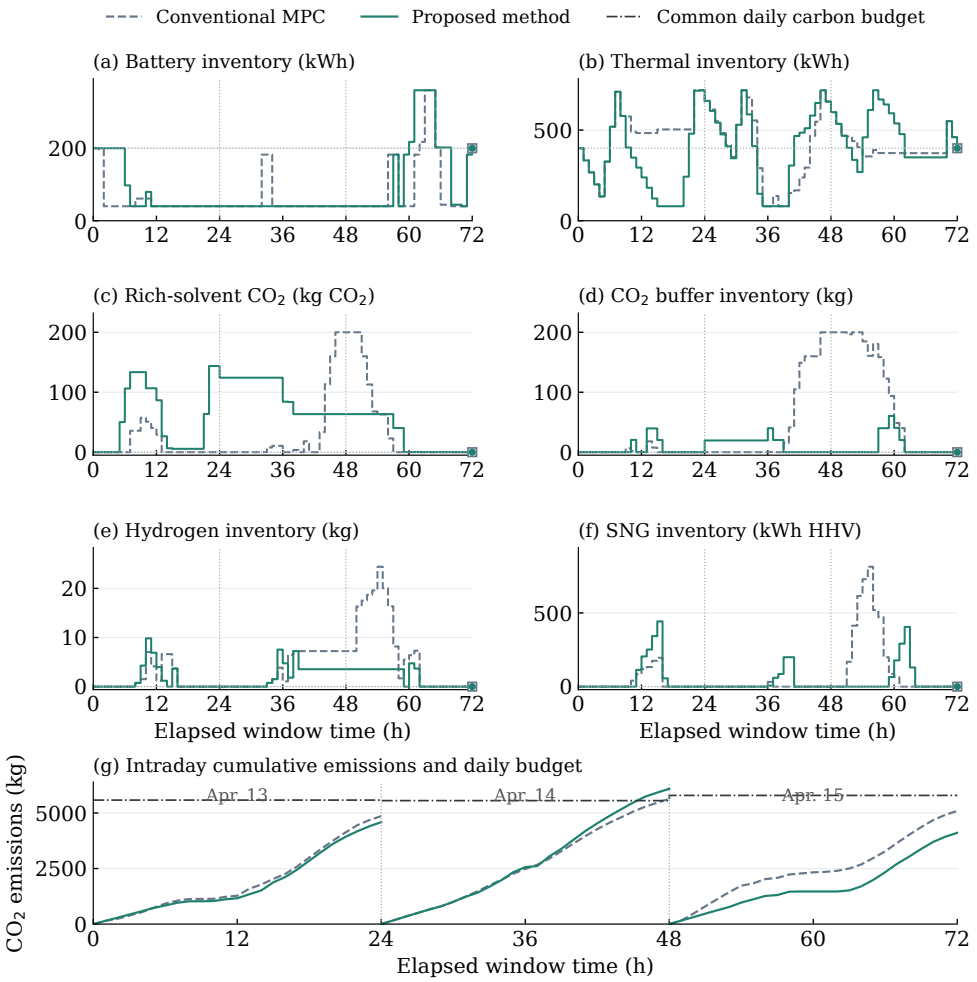

Fig. 5 Inventory transitions, intraday cumulative emissions, and terminal restoration over the complete April 13–15, 2009 window. Vertical dotted lines denote day boundaries, horizontal dotted lines in inventory panels show common terminal targets, and endpoint markers at 72 h show solved inventories. Cumulative emissions reset daily and budgets update by day. All six initial and final inventory targets are identical.

5.4 Sensitivity to equipment capacity and budget parameters

Capacity multipliers of 0.5/1/2 and budget-reference ratios of 0.90/0.95/1.00 form a complete 3×3 grid. Additional cases use the official annual factor of 0.449 and the original PV multiplier of one. Four fixed development days with 24-h hard terminal constraints yield 88 runs for the two methods. Initial and terminal inventories scale consistently with capacity. These analyses are reported separately from the 72-day consecutive-operation validation.

Across the nine capacity–budget cases, the proposed method increases operating expenditure by approximately 0.20%–0.36%, reduces operational CO_2 emissions by approximately 0.48%–0.58%, and increases end-to-end computation time by approximately 11.9%–29.3% relative to conventional MPC. Expenditure decreases by approximately 0.04% with the annual factor of 0.449 and increases by approximately 0.34% under the original PV capacity.

The monthly quantile correction is recalibrated when the budget-reference ratio changes. These cases therefore describe performance under changing engineering parameters; interpretation of budget tightness and coordination mechanisms is discussed in Sect. 6.

5.5 Operating boundaries of the closed carbon cycle

A marginal analysis across equipment loads examines the complete chain of capture, regeneration, electrolytic hydrogen production, methanation, and final combustion. The functional unit is 1 kg of CO_2 processed, with identical initial and final inventories to exclude temporary benefits from net inventory depletion. Methanation throughput q is sampled at 151 equally spaced points from 20.25 to 45 kg CO_2/h, corresponding to 45%–100% load. The fraction f of recoverable methanation heat that actually replaces boiler heating is 0, 0.5, or 1, yielding 453 operating points. The analysis assumes warm, steady-state operation and excludes startup transients and capital investment.

In the original model, electrolyzer power is $P_{\mathrm{EL}} = 54(8/44)q + 9.0909$ kW. Allocating fixed idle demand over actual throughput and adding hydrogen-compression, absorption, and regeneration auxiliary consumption gives $e(q) = 10.15 + 9.0909/q$. Figure 6(a) shows a declining specific electricity demand with diminishing sensitivity as load increases. The nonlinearity follows directly from fixed idle-power allocation, without an additional fitted efficiency curve. Increasing load from 45% to 100% reduces total specific electricity consumption from 10.5989 to 10.3520 kWh/kg CO_2, approximately 2.33%. On a common HHV fuel-energy basis, the change in net purchased fossil fuel is

$$\begin{aligned} e(q) &= 10.15 + 9.0909/q, \\ \Delta F(f) &= h_{\mathrm{reg}}/\eta_{\mathrm{reg}} - g_{\mathrm{SNG}} - fQ_{\mathrm{MR}}/\eta_{\mathrm{heat}}. \end{aligned} \tag{31}$$

Here, q is in kg CO_2/h, $e(q)$ in kWh/kg CO_2, and $\Delta F(f)$ in kWh HHV/kg CO_2. Regeneration heat is $h_{\mathrm{reg}} = 1$ kWh/kg CO_2 and regenerator efficiency is $\eta_{\mathrm{reg}} = 0.90$. Synthetic-methane yield is $g_{\mathrm{SNG}} = 5.60606$ kWh HHV/kg CO_2, recoverable methanation heat is $Q_{\mathrm{MR}} = 0.72917$ kWh/kg CO_2, and marginal boiler efficiency is $\eta_{\mathrm{heat}} = 0.93$. Because Q_{MR} already includes the 70% recovery factor, f denotes only

the fraction actually replacing boiler heat; recovery is not counted twice. The reference gas price is $p_f = 0.19820$ CNY/kWh HHV and gas emissions factor is $e_{\text{gas}} = 0.178378$ kg CO_2/kWh HHV. Benefits arise through reduced fossil-gas purchases; emissions from final SNG combustion remain in the carbon account.

Additional nonenergy O&M is represented by $c_{\text{add}}(q) = a + b/q$. The specified endpoint values, 0.70563 and 0.70458 CNY/kg CO_2 at minimum and full load, give $a = 0.70372091$ and $b = 0.03865909$. This expression reconstructs an O&M relationship consistent with both endpoints. Unused recoverable heat incurs the heat-rejection tariff of 0.0021212 CNY/kWh, giving $c_{\text{rej}}(f) = 0.0021212(1 - f)Q_{\text{MR}}$ CNY/kg CO_2. Electricity consumption, fuel substitution, and O&M jointly determine the emissions and economic thresholds; currency conversion follows Sect. 4.2.

Let λ be marginal electricity carbon intensity in kg CO_2/kWh and p_e the electricity opportunity cost in CNY/kWh. Relative to providing identical final energy services without adding this recycling chain, the marginal operational-emissions change ΔC and cash operating-expenditure change ΔJ per functional unit are

$$\begin{aligned} \Delta C(q, f) &= \lambda e(q) + e_{\text{gas}} \Delta F(f), \\ \Delta J(q, f) &= p_e e(q) + p_f \Delta F(f) + c_{\text{add}}(q) + c_{\text{rej}}(f). \end{aligned} \tag{32}$$

The units of ΔC and ΔJ are kg CO_2/kg CO_2 processed and CNY/kg CO_2 processed, respectively; negative values indicate emissions reductions and savings. The quantity ΔJ includes energy purchases, additional nonenergy O&M, and heat rejection, but excludes carbon shadow costs and budget-slack penalties. With inventory closure, carbon consumed in methanation is not deducted again as permanent sequestration. Equation (32) gives simultaneous emissions reductions and savings when

$$\begin{aligned} \lambda < \lambda_{\text{crit}}(q, f) &= \frac{-e_{\text{gas}} \Delta F(f)}{e(q)}, \\ p_e < p_{e,\text{crit}}(q, f) &= \frac{-[p_f \Delta F(f) + c_{\text{add}}(q) + c_{\text{rej}}(f)]}{e(q)}. \end{aligned} \tag{33}$$

The thresholds λ_{crit} and $p_{e,\text{crit}}$ are upper limits on electricity carbon intensity and opportunity cost, respectively; equality corresponds to marginal break-even operation. To compare load effects, Figs. 6(b) and 6(c) use the threshold at 45% load ($q = 20.25$ kg CO_2/h) under each heat-utilization condition as the baseline and define relative gains as

$$\begin{aligned} r_\lambda(q, f) &= \left[\frac{\lambda_{\text{crit}}(q, f)}{\lambda_{\text{crit}}(20.25, f)} - 1 \right] \times 100\%, \\ r_p(q, f) &= \left[\frac{p_{e,\text{crit}}(q, f)}{p_{e,\text{crit}}(20.25, f)} - 1 \right] \times 100\%. \end{aligned} \tag{34}$$

Figure 6 is computed pointwise from Eqs. (31)–(34). Increasing load from 45% to 100% decreases specific electricity consumption by approximately 2.33% and raises the emissions threshold by approximately 2.39%; normalized emissions-threshold curves coincide for all three values of f. Relative economic-threshold gains are approximately 2.970%, 2.795%, and 2.701% for $f = 0$, 0.5, and 1, respectively. The declining relative gain with increasing f reflects different baseline thresholds and does not imply that

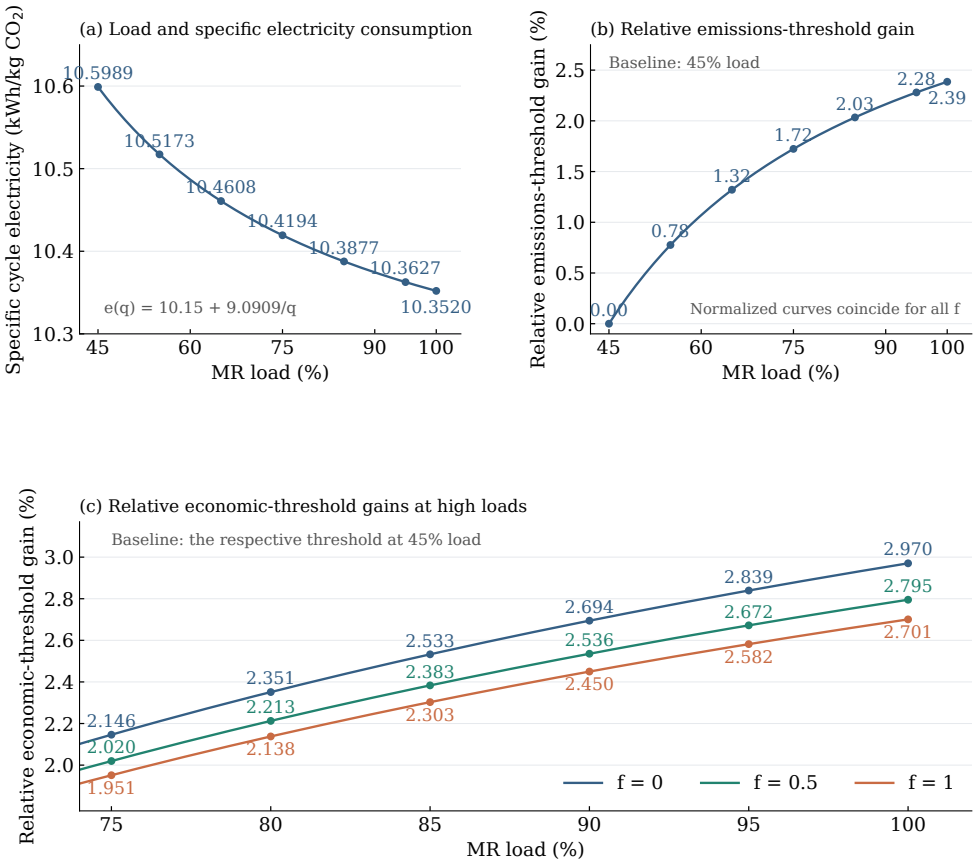

Fig. 6 Specific electricity consumption and operating thresholds of the inventory-closed carbon cycle. (a) Specific cycle electricity consumption. (b) Relative emissions-threshold gain from the 45%-load baseline; normalized curves coincide for all three values of f. (c) Relative economic-threshold gain at 75%–100% load, measured against the respective 45%-load baseline. The parameter f is the fraction of recoverable methanation heat that actually replaces boiler heating. Nodes are evaluated directly from the equations; the axes in panel (c) are restricted to show the actual differences.

heat utilization reduces economic performance. At full load, the absolute emissions thresholds are approximately 0.07745 and 0.09096 kg CO_2/kWh for $f = 0$ and 1; the corresponding economic thresholds are approximately 0.01785 and 0.03301 CNY/kWh.

Equation (33) identifies the electricity-supply conditions required for the closed cycle to reduce both emissions and expenditure. The annual grid factor of 0.31 kg CO_2/kWh and minimum reference tariff of 0.5851 CNY/kWh in Sect. 4.2 both lie outside these thresholds. Under this parameter scenario, recycling should therefore be matched primarily to low-carbon surplus electricity with a low opportunity cost. Effective heat utilization further expands the feasible operating region by replacing boiler fuel. Closed-cycle marginal analysis identifies operating conditions, whereas overall multidevice benefits are evaluated from executed trajectories.

6 Discussion and Scope of Applicability

Under common equipment, inventory-closure, and daily-budget conditions, the overall scheme reduces aggregate operating expenditure and operational CO_2 emissions over the 72 tested days. Computational effort, window-to-window variation, and engineering sensitivity are reported in Table 4, Fig. 2, and Sect. 5.4, respectively. The methods have equal numbers of budget-compliant days, and the interval for the budget-exceedance difference spans zero. Budget-related results are interpreted within this statistical scope; average economic and emissions improvements are the principal empirical findings.

Conventional MPC and the proposed method share dynamic carbon-inventory constraints and daily-budget propagation, so the comparison evaluates scenario treatment and trajectory reuse together. The joint economic-quality certificate bounds candidate finite-horizon objective error; executed expenditure and actual compliance are evaluated separately from operating trajectories. Closed-loop stability requires additional theoretical conditions. The current certificate acceptance rate is 6.25%. Further work can reduce candidate-construction and bound-evaluation overhead and isolate individual coordination mechanisms within the same scenario optimization problem.

The model uses inventory-level dynamic approximations suitable for hourly dispatch. Added capacities, heat/cooling rejection limits, and startup energies are engineering assumptions. Process-level validation of absorber/reboiler thermal inertia, electrolyzer auxiliary consumption, and methanation cold starts and heat maintenance can draw on thermodynamic capture models (Weimann et al. 2023), electrolyzer economic MPC (Huang et al. 2022), P2G thermoeconomic analysis (Calise et al. 2024), and validated dynamic models of energy systems with P2G plants (Prabhakaran et al. 2023). The present analysis covers operational expenditure and emissions; equipment investment, life-cycle assessment, and coupling with demand response and carbon trading are possible extensions.

7 Conclusions

A six-inventory dynamic model for rich solvent, buffered CO_2, hydrogen, SNG, battery energy, and thermal energy consistently describes electricity–heat–cooling–gas balances and device coupling. Capture, regeneration, hydrogen production, methanation, and subsequent combustion share one energy and carbon accounting boundary. Day-ahead scheduling and intraday receding-horizon optimization jointly track realized emissions, the remaining daily budget, and inventories. A joint economic-quality certificate tests the finite-horizon objective quality of candidate trajectory reuse.

Across 24 prespecified three-day windows in 2009–2010, totaling 72 operating days, the proposed method reduces aggregate operating expenditure by approximately 0.81%, or approximately 8325 CNY, and operational CO_2 emissions by approximately 0.84% relative to conventional MPC. All 108 accepted candidates pass original-constraint and independent upper/lower-bound checks. Both methods restore common inventory targets at the end of every window, so the reported cycle benefits are evaluated under inventory closure.

Closed-cycle marginal analysis quantifies the effects of equipment load and effective heat utilization on operating thresholds. Raising methanation load from 45% to 100% reduces specific cycle electricity consumption by approximately 2.33%. Greater effective heat utilization raises the absolute emissions and economic thresholds, providing a quantitative basis for carbon recycling and multiday energy–carbon coordination with low-carbon electricity at a low opportunity cost.

Statements and declarations

Conflict of interest

The authors declare no conflicts of interest.

Ethics approval

Ethics approval was not required for this study, which involved computational modeling and analysis of publicly available energy-metering data and did not involve human participants or animal subjects.

Author contributions

Junjie He: Methodology; Software; Formal analysis; Writing – original draft.
Zhigang Zhang: Conceptualization; Supervision.

Data availability

The original hourly energy-metering data are publicly available from the Kitakyushu dataset described by Liao et al. (2024b). The dataset itself is archived on figshare with DOI 10.6084/m9.figshare.24978645 (Liao et al. 2024a). The processed input data, optimization code, and archived operating trajectories used in this study are available from the corresponding author upon reasonable request.

References

Angeli D, Amrit R, Rawlings JB (2012) On Average Performance and Stability of Economic Model Predictive Control. IEEE Transactions on Automatic Control 57(7):1615–1626. https://doi.org/10.1109/TAC.2011.2179349

Buttler A, Spliethoff H (2018) Current status of water electrolysis for energy storage, grid balancing and sector coupling via power-to-gas and power-to-liquids: A review. Renewable and Sustainable Energy Reviews 82:2440–2454. https://doi.org/10.1016/j.rser.2017.09.003

Calise F, Cappiello FL, Cimmino L, et al (2024) Dynamic analysis and thermoeconomic optimization of a Power-to-Gas system driven by renewables. Energy Conversion and Management 313:118647. https://doi.org/10.1016/j.enconman.2024.118647

Campi MC, Garatti S (2008) The Exact Feasibility of Randomized Solutions of Uncertain Convex Programs. SIAM Journal on Optimization 19(3):1211–1230. https://doi.org/10.1137/07069821X

Chan LLT, Chen J (2018) Economic model predictive control of an absorber-stripper CO2 capture process for improving energy cost. IFAC-PapersOnLine 51(18):109–114. https://doi.org/10.1016/j.ifacol.2018.09.284

Dolan ED, Moré JJ (2002) Benchmarking optimization software with performance profiles. Mathematical Programming 91(2):201–213. https://doi.org/10.1007/s101070100263

Fan G, Peng C, Wang X, et al (2024) Optimal scheduling of integrated energy system considering renewable energy uncertainties based on distributionally robust adaptive MPC. Renewable Energy 226:120457. https://doi.org/10.1016/j.renene.2024.120457

Gao C, Lu H, Chen M, et al (2025) A low-carbon optimization of integrated energy system dispatch under multi-system coupling of electricity-heat-gas-hydrogen based on stepwise carbon trading. International Journal of Hydrogen Energy 97:362–376. https://doi.org/10.1016/j.ijhydene.2024.11.055

Giglio E, Pirone R, Bensaid S (2021) Dynamic modelling of methanation reactors during start-up and regulation in intermittent power-to-gas applications. Renewable Energy 170:1040–1051. https://doi.org/10.1016/j.renene.2021.01.153

Götz M, Lefebvre J, Mörs F, et al (2016) Renewable Power-to-Gas: A technological and economic review. Renewable Energy 85:1371–1390. https://doi.org/10.1016/j.renene.2015.07.066

He D, Tian Y, Du H (2023) Event-triggered economic MPC with relaxed contractive constraints. Journal of Process Control 127:102992. https://doi.org/10.1016/j.jprocont.2023.102992

Herrmann F, Grünewald M, Meijer T, et al (2022) Operating window and flexibility of a lab-scale methanation plant. Chemical Engineering Science 254:117632. https://doi.org/10.1016/j.ces.2022.117632

Huang C, Zong Y, You S, et al (2022) Economic model predictive control for multi-energy system considering hydrogen-thermal-electric dynamics and waste heat recovery of MW-level alkaline electrolyzer. Energy Conversion and Management 265:115697. https://doi.org/10.1016/j.enconman.2022.115697

International Energy Agency (2019) Putting CO_2 to Use: Creating Value from Emissions. Tech. rep., International Energy Agency, URL https://www.iea.org/reports/putting-co2-to-use, published September 25, 2019; accessed November 6, 2026

Jiang Y, Ren Z, Li W (2024) Committed Carbon Emission Operation Region for Integrated Energy Systems: Concepts and Analyses. IEEE Transactions on Sustainable Energy 15(2):1194–1209. https://doi.org/10.1109/TSTE.2023.3330857

Kumar R, Wenzel MJ, ElBsat MN, et al (2020) Stochastic model predictive control for central HVAC plants. Journal of Process Control 90:1–17. https://doi.org/10.1016/j.jprocont.2020.03.015

Kyushu Electric Power (2025) Energy and Environmental Plan for FY2025. URL https://www.kyuden.co.jp/var/rev0/0846/2994/ene_plan_2025.pdf, in Japanese; translated title; provisional FY2024 emissions factors, p. 1; accessed November 6, 2026

Kyushu Electric Power (n.d.) Business Seasonal and Time-of-Use Electricity Tariff A-I. URL https://www.kyuden.co.jp/business/menu/menu-select/mainland/gyomukijia-1.html, in Japanese; translated title; earlier schedule labeled through October 31; accessed November 6, 2026

Liao W, Jin X, Li Y (2024a) 20-year Data of Energy Station at Kitakyushu Campus. figshare (dataset), https://doi.org/10.6084/m9.figshare.24978645, URL https://figshare.com/articles/dataset/Energy_Station_Data/24978645, accessed November 6, 2026

Liao W, Jin X, Ran Y, et al (2024b) A twenty-year dataset of hourly energy generation and consumption from district campus building energy systems. Scientific Data 11(1):1400. https://doi.org/10.1038/s41597-024-04244-6

Liu G, Han D, Liu C, et al (2023) Dual time scale optimal scheduling of integrated energy system considering dual demand response and stepped carbon trading. Electric Power Automation Equipment 43(5):218–225. https://doi.org/10.16081/j.epae.202210008, in Chinese

Liu H, Niu H, Ma Q, et al (2026) Multi-Time-Scale Power and Energy Balance Optimization Method for Power Systems Considering Hydrogen Energy Storage Failures Under Dynamic Carbon Quota Allocation. Energies 19(19):4728. https://doi.org/10.3390/en19194728

Marzi E, Morini M, Saletti C, et al (2024) Coordinating multiple Power-To-Gas plants for optimal management of e-fuel seasonal storage. Smart Energy 14:100143. https://doi.org/10.1016/j.segy.2024.100143

Mayne DQ, Rawlings JB, Rao CV, et al (2000) Constrained model predictive control: Stability and optimality. Automatica 36(6):789–814. https://doi.org/10.1016/S0005-1098(99)00214-9

Pavlov A, Shames I, Manzie C (2019) Early Termination of NMPC Interior Point Solvers: Relating the Duality Gap to Stability. In: 2019 18th European Control Conference (ECC). IEEE, pp 805–810, https://doi.org/10.23919/ECC.2019.8795629

Prabhakaran P, Graf F, Koeppel W, et al (2023) Modelling and validation of energy systems with dynamically operated Power to Gas plants for gas-based sector coupling in de-central energy hubs. Energy Conversion and Management 276:116534. https://doi.org/10.1016/j.enconman.2022.116534

Qiu R, Wang Q, Tang Z, et al (2025) Economic and flexible operation of solvent-based carbon capture system with solvent storage based on absorption-desorption decentralized predictive control. Energy 336:138178. https://doi.org/10.1016/j.energy.2025.138178

Saibu Gas (n.d.) Average Prices of Large-Volume Gas Tariffs. URL https://www.saibugas.co.jp/business/rates/pdf/h28_oogchi.pdf, in Japanese; translated title; FY2016 results, pretax at 45 MJ/m^3; accessed November 6, 2026

Schiebahn S, Grube T, Robinius M, et al (2015) Power to gas: Technological overview, systems analysis and economic assessment for a case study in Germany. International Journal of Hydrogen Energy 40(12):4285–4294. https://doi.org/10.1016/j.ijhydene.2015.01.123

Schildbach G, Fagiano L, Frei C, et al (2014) The scenario approach for Stochastic Model Predictive Control with bounds on closed-loop constraint violations. Automatica 50(12):3009–3018. https://doi.org/10.1016/j.automatica.2014.10.035

Shi Z, Yang Y, Xu Q, et al (2023) A low-carbon economic dispatch for integrated energy systems with CCUS considering multi-time-scale allocation of carbon allowance. Applied Energy 351:121841. https://doi.org/10.1016/j.apenergy.2023.121841

State Administration of Foreign Exchange (2026) RMB Central Parity Rates. URL https://www.safe.gov.cn/AppStructured/hlw/RMBQuery.do, November 2, 2026 record: 100 JPY = 4.2424 CNY; accessed November 6, 2026

Sternberg A, Bardow A (2015) Power-to-What? – Environmental assessment of energy storage systems. Energy & Environmental Science 8(2):389–400. https://doi.org/10.1039/C4EE03051F

U.S. Department of Energy (n.d.) Technical Targets for Proton Exchange Membrane Electrolysis. URL https://www.energy.gov/cmei/fuels/technical-targets-proton-exchange-membrane-electrolysis, accessed November 6, 2026; 2022 system-status values

Weimann L, Dubbink G, van der Ham L, et al (2023) A thermodynamic-based mixed-integer linear model of post-combustion carbon capture for reliable use in energy system optimisation. Applied Energy 336:120738. https://doi.org/10.1016/j.apenergy.2023.120738

Zhang G, Wang W, Chen Z, et al (2022) Modeling and optimal dispatch of a carbon-cycle integrated energy system for low-carbon and economic operation. Energy 240:122795. https://doi.org/10.1016/j.energy.2021.122795

Zhang J, Liu S, Liu J (2014) Economic model predictive control with triggered evaluations: State and output feedback. Journal of Process Control 24(8):1197–1206. https://doi.org/10.1016/j.jprocont.2014.03.009